ACS APPLIED NANO MATERIALS

www.acsanm.org Article

Mapping Elevated Temperatures with a Micrometer Resolution Using the Luminescence of Chemically Stable Upconversion Nanoparticles

Thomas P. van Swieten, Tijn van Omme, Dave J. van den Heuvel, Sander J.W. Vonk, Ronald G. Spruit, Florian Meirer, H. Hugo Pérez Garza, Bert M. Weckhuysen, Andries Meijerink,* Freddy T. Rabouw,* and Robin G. Geitenbeek

Cite This: *ACS Appl. Nano Mater.* 2021, 4, 4208–4215 Read Online

ACCESS | Metrics & More | Article Recommendations | Supporting Information

ABSTRACT: The temperature-sensitive luminescence of nanoparticles enables their application as remote thermometers. The size of these nanothermometers makes them ideal to map temperatures with a high spatial resolution. However, high spatial resolution mapping of temperatures >373 K has remained challenging. Here, we realize nanothermometry with high spatial resolutions at elevated temperatures using chemically stable upconversion nanoparticles and confocal microscopy. We test this method on a micro-electromechanical heater and study the temperature homogeneity. Our experiments reveal distortions in the luminescence spectra that are intrinsic to high-resolution measurements of samples with nanoscale photonic inhomogeneities. In particular, the spectra are affected by the high-power excitation as well as by scattering and reflection of the emitted light. The latter effect has an increasing impact at elevated temperatures. We present a procedure to correct these distortions. As a result, we extend the range of high-resolution nanothermometry beyond 500 K with a precision of 1−4 K. This work will improve the accuracy of nanothermometry not only in micro- and nanoelectronics but also in other fields with photonically inhomogeneous substrates.

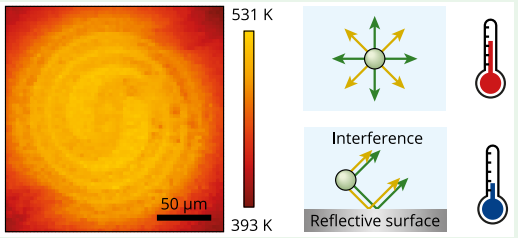

KEYWORDS: *nanothermometry, luminescence, temperature mapping, microscopy, spectral artifacts, photonics*

INTRODUCTION

Thermometry on the microscopic scale is an essential characterization tool for the development of nano- and microelectronic devices.[1−4] However, conventional thermometers like thermocouples are often unable to reliably measure the temperature on this length scale due to their size. An additional drawback is the requirement of direct contact between the sensing element and the temperature-registration instrument. The development of remote temperature sensing by optical thermometry techniques partially solved this issue. These techniques rely on temperature-dependent blackbody radiation (infrared thermography),[5] Raman scattering,[6,7] reflectance,[8] luminescence,[9] or other optical properties.[10] Thermometry based on luminescence is particularly interesting since it is easily implemented, requiring only the deposition of a luminescent material in or on a sample of interest and the detection of its luminescence. The development of bottom-up synthesis methods for luminescent materials with nanoscale dimensions opened up the field of luminescence nanothermometry[11] with a dramatically enhanced spatial resolution. Therefore, luminescence nanothermometry is currently developing into the method of choice for temperature measurements in microscopy.[12−16]

Several luminescence properties of a nanothermometer can serve as a measure of temperature. The luminescence intensity ratio (LIR) between two emission bands is a popular choice because it is generally considered insensitive to experimental parameters such as excitation intensity, alignment, or the amount of deposited thermometer material. Typical nanothermometers used in LIR thermometry consist of an inorganic host crystal doped with lanthanide (Ln^{3+}) ions, which become luminescent due to 4f−4f transitions. The minor spectral overlap between these transitions and their narrow linewidth prevents systematic errors and provides high accuracy in the determination of the LIR. An additional advantage of Ln^{3+}-doped nanocrystals is the possibility to efficiently generate upconversion luminescence, that is, the emission of one high-energy photon after the absorption of at least two low-energy photons.[17,18] Via this process, infrared excitation can lead to visible luminescence. While detection of visible luminescence

Received: March 7, 2021
Accepted: March 15, 2021
Published: March 30, 2021

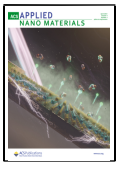

https://doi.org/10.1021/acsanm.1c00657
ACS Appl. Nano Mater. 2021, 4, 4208−4215

is straightforward with a standard camera or a photodiode, excitation with infrared light prevents background fluorescence, a common issue of conventional down-shifting luminescence, that is, excitation with one high-energy photon resulting in the emission of one low-energy photon. These properties of upconversion nanoparticles guarantee accurate determination of the LIR and thus reliable temperature measurements.

Typical applications of upconversion nanoparticles in thermometry on the microscopic scale are in cell biology and microelectronics. Upconversion luminescence from Er^{3+}/Yb^{3+}-doped nanoparticles is well known for temperature mapping in these fields,[12,13,16] but Eu^{3+}/Tb^{3+}- and Eu^{3+}/Sm^{3+}-doped systems have also been used.[14,15] Using these nanoparticles, a high spatial resolution is achieved by spatially mapping the LIR using either wide-field or confocal microscopy. Thermometry via wide-field microscopy is a fast technique as it directly images the intensity maps of two emission bands using bandpass filters. Dividing the two images yields the spatially resolved LIR, which easily translates to a temperature map. Confocal microscopy is a slower technique as a laser spot scans the sample to construct an image. However, it can provide a spectrum for every pixel enabling a more reliable determination of the LIR. Both techniques are mainly used to probe temperatures up to ~350 K. Recent work by our group demonstrated that it is possible to extend the temperature range to 873 K using luminescent microcrystals.[3] In this previous work, deposition of the microcrystals on a microheater designed for in situ transmission electron microscopy (TEM) experiments revealed a temperature profile with a spatial resolution of roughly 10 μm. However, these microheaters and other microelectromechanical systems (MEMS) contain structures with dimensions smaller than 1 μm.[19] A higher spatial resolution of luminescence thermometry at elevated temperatures is thus crucial for its implementation in MEMS technology.

In this work, we develop a combined microscopy and data analysis approach to map elevated temperatures with a high spatial resolution. In particular, we measure the local temperatures on a MEMS-based microheater using confocal microscopy mapping of the two green emission bands of $NaYF_4:Er^{3+},Yb^{3+}$ upconversion nanoparticles. The demand for a high spatial resolution comes with intrinsic challenges due to the higher excitation powers necessary to obtain a sufficient signal[20,21] and due to inhomogeneities of the optical environment of nanothermometers. We characterize both phenomena and develop data analysis procedures to correct them. This enables a quantitative study of the temperature profile generated by the microheater at elevated temperatures up to 523 K.

EXPERIMENTAL SECTION

Sample Preparation. The synthesis procedure reported in the work of Geitenbeek et al. was used to obtain multiple batches of $NaYF_4:Er^{3+}(2\%),Yb^{3+}(18\%)$ nanoparticles dispersed in cyclohexane.[17] Deposition of the nanoparticles was achieved by drop casting on a microheater (Wildfire Nano-Chips, commercially available from DENSsolutions). The thickness of the dried nanoparticle layer (a few μm) was estimated using the concentration of the nanoparticle dispersion. Microcrystalline $NaYF_4:Er^{3+}(2\%),Yb^{3+}(18\%)$ samples were obtained following the procedure of Krämer et al.[22]

Characterization. The particle size and morphology were investigated using an FEI Tecnai 12 transmission electron microscope operating at 120 keV. Samples were prepared by drying the diluted nanoparticle dispersion onto carbon-coated copper grids. The luminescence of the dried nanoparticle layer was mapped using a Nikon TE2000-S inverted microscope fitted with a C1si confocal scanner.[23] A 980 nm laser diode was connected to the confocal scanner head using a single-mode fiber. The laser light was reflected using a 680 nm shortpass dichroic mirror and focused on the nanoparticle layer using a 10× CFI Plan Fluor (NA = 0.3) air objective or a 40× CFI S Plan Fluor ELWD (NA = 0.6) air objective. The luminescence was directed back to the confocal scanner head by the same objective, passed through the dichroic mirror, coupled into a 50 μm multimode fiber, passed through a 680 nm shortpass filter, dispersed by an equilateral SF10 glass prism (Linos), and finally detected using a back-illuminated CCD (Princeton Instruments, NTE/CCD-1340). All maps were obtained with a pixel dwell time of 100 ms. For the calibration of the luminescence, powders of dried nanoparticles were heated with a Linkam THMS600 microscope stage. Selective excitation of the microcrystalline $NaYF_4:Er^{3+}(2\%),Yb^{3+}(18\%)$ sample with 404 and 448 nm light was carried out using an Edinburgh Instruments FLS920 spectrofluorometer equipped with TMS300 monochromators, a R928 photomultiplier tube, and a Xe lamp (450 W). The reflection measurements were performed on a Nikon Ti-U inverted microscope. The microheater was illuminated in wide field with a broad-spectrum LED (Lumencor Sola) by a 40× Nikon CFI Plan Fluor (NA = 0.75) air objective. The reflected light was collected by the same objective and collimated outside of the microscope using a relay lens system. The light was focused on a mechanical slit at the entrance of an Andor Kymera 193i spectrometer and dispersed with a 150 lines/mm grating on an Andor iXon EMCCD.

Simulation. Finite element simulations were carried out using COMSOL Multiphysics. The electric currents and heat transfer modules were two-way coupled to include the temperature-dependent resistivity. The model assumes a vacuum environment. Convective heat transfer through air is not taken into account, but radiation is included. The validity of the model was shown in our previous work.[24]

RESULTS AND DISCUSSION

The microheater consists of a spiral-shaped metal that is embedded between two layers of silicon nitride that form a membrane (Figure 1a,b).[24] A silicon substrate supports the membrane with the microheater and enables loading into a dedicated TEM holder. Four metal needles connect the holder with the metal contacts of the microheater. By applying a voltage across two of the contacts, a current flows, which induces Joule heating. The two other contacts are used to measure resistance. The metal has a linear relationship between resistance and temperature, which is exploited to measure and control the temperature. Figure 1c shows the temperature profile at a center temperature of 523 K as predicted by a finite element model.[24] The geometry of the metal spiral was designed to generate a homogeneous temperature in the center area where the electron microscopy users place their samples. Outside this area, over a distance of 175 μm between the heating spiral and the silicon substrate, the temperature shows a steep gradient to room temperature at the edges of the membrane. This is explained by the low thermal conductivity of silicon nitride, which minimizes heat loss through the membrane. The much higher thermal conductivity of the silicon substrate ensures that the substrate remains at room temperature. Measuring the gradient requires a thermometry technique with a high spatial resolution.

Calibration of the resistance−temperature relation of the heater is currently done using Raman spectroscopy. Silicon particles are deposited on the microheater, which is inserted into a vacuum chamber to imitate the conditions of an electron microscopy experiment. The position of the silicon peak in the

https://doi.org/10.1021/acsanm.1c00657
ACS Appl. Nano Mater. 2021, 4, 4208−4215

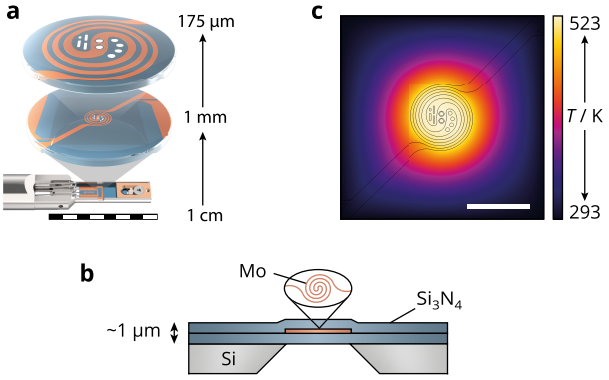

Figure 1. A microheater for an in situ TEM experiment. (a) Magnification of the microheater design. The metal heating spiral (orange) is embedded in a silicon nitride membrane (blue). Electron microscopy users place their samples on the electron-transparent silicon nitride windows in the center of the heater. The scale bar is 1 cm, 1 mm, and 175 μm for the bottom, middle, and top magnification, respectively. (b) Side view of the microheater. A silicon substrate supports the silicon nitride membrane with the encapsulated molybdenum heating spiral. Due to its low thermal conductivity, silicon nitride acts as a thermal insulator between the heater and the silicon substrate. This way a steep temperature gradient is realized between the edge of the heating spiral and the 400 μm-thick silicon substrate, which remains at room temperature. (c) Temperature profile across the membrane and the microheater for a center temperature of 523 K simulated with a finite element model. The scale bar is 175 μm.

Raman spectrum around 520 cm^{-1} is used as a measure of temperature.[6,25] Although the size of the Raman laser spot (1 μm) guarantees a high spatial resolution, the temperature uncertainty can be as high as 13 K at 523 K.[24] The aim of our luminescence thermometry technique is thus to measure temperature with a similar spatial resolution but a lower temperature uncertainty.

The discussion of our technique starts with the characterization of the luminescent thermometers. We use hexagonal $NaYF_4$ nanoparticles doped with 2% Er^{3+} and 18% Yb^{3+}. The choice of this specific composition is motivated by its relatively high upconversion quantum yield.[26] Using a colloidal synthesis procedure,[17] we first produce cubic α-$NaYF_4$:Er^{3+}(2%),Yb^{3+}(18%) nanoparticles and further heat these to 573 K to obtain hexagonal β-$NaYF_4$:Er^{3+}(2%),Yb^{3+}(18%) nanoparticles with a diameter of 32 ± 1 nm (Figure 2a,b). Excitation with 980 nm light yields bright green upconversion emission due to the radiative transitions in Er^{3+} from the thermally coupled $^2H_{11/2}$ and $^4S_{3/2}$ levels to the $^4I_{15/2}$ ground state (Figure 2c). Thermal coupling between these levels leads to stronger luminescence from the higher-excited level upon a temperature (T) increase, which follows Boltzmann statistics[27]

$$\frac{I_2}{I_1} = \frac{A_2 g_2}{A_1 g_1} \exp\left(\frac{-\Delta E}{k_B T}\right) = C \exp\left(\frac{-\Delta E}{k_B T}\right) \quad (1)$$

where k_B is the Boltzmann constant and ΔE is the energy difference between the thermally coupled levels. I_i and A_i are the integrated luminescence intensity and the spontaneous emission rate from excited state i to the ground state with degeneracy g_i, respectively. If ΔE is known (for example from the literature), one could extract the exponential prefactor C from the intensity ratio in an emission spectrum. However, such a "calibration-free" procedure introduces an additional error. We therefore fit the LIR between the $^2H_{11/2}$ and $^4S_{3/2}$ emissions at various temperatures to the Boltzmann model in eq 1 and find a ΔE value of 759 cm^{-1} (Figure 2d), which is in agreement with ΔE values from the literature.[17] This model can thus serve as calibration for our thermometers to accurately measure temperature.

As nanothermometry requires high excitation intensities to obtain a sufficient signal, we must understand how not only temperature but also intense excitation changes the upconversion emission spectrum (Figure 3a). We observe an upconversion emission band at 555 nm that becomes stronger with the increasing excitation intensity. With reference measurements, upon excitation into (404 nm) or just below (448 nm) the $^2H_{9/2}$ state of Er^{3+} (Figure 3b), we can show that the 555 nm emission must be due to radiative relaxation from the $^2H_{9/2}$ state to the first-excited state ($^4I_{13/2}$) of Er^{3+}. The

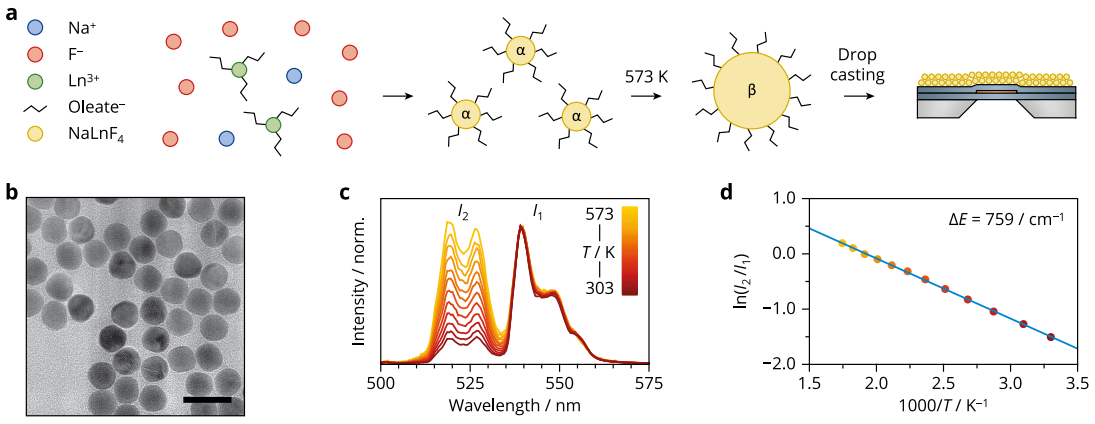

Figure 2. Upconversion nanoparticles: their fabrication and luminescence. (a) Schematic of the two-step synthesis of the nanoparticles—small cubic α-$NaLnF_4$ (Ln^{3+} = Y^{3+}, Er^{3+}, or Yb^{3+}) particles form at room temperature followed by growth to larger β-$NaLnF_4$ particles at 573 K. These particles are deposited on the microheater by drop casting. (b) TEM image of $NaYF_4$:Er^{3+}(2%),Yb^{3+}(18%) nanoparticles with a diameter of 32 ± 1 nm. The scale bar is 50 nm. (c) Green upconversion luminescence of the nanoparticles upon 980 nm excitation (1.0 kW cm^{-2}) at various temperatures ranging from 303 K (dark red) to 573 K (yellow). (d) The logarithm of the ratio between the integrated intensities from (c) vs the reciprocal temperature (colored dots). The integration boundaries for the $^2H_{11/2}$ and $^4S_{3/2}$ emissions are 510−530 nm and 537−560 nm, respectively. The blue line is a fit of the experimental ratios to the Boltzmann model of eq 1.

https://doi.org/10.1021/acsanm.1c00657
ACS Appl. Nano Mater. 2021, 4, 4208−4215

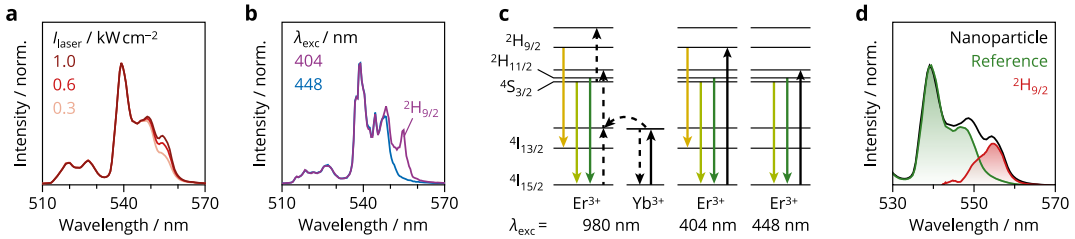

Figure 3. Multiphoton upconversion. (a) Green upconversion luminescence of the nanoparticles at different excitation intensities of the 980 nm laser. (b) Emission spectra of a microcrystalline $NaYF_4$:Er^{3+}(2%),Yb^{3+}(18%) sample at different excitation wavelengths recorded with a high spectral resolution using a spectrofluorometer. (c) Simplified energy level diagrams for three different excitation wavelengths with the absorption, emission, and energy transfer transitions indicated by solid black, solid-colored, and dashed black arrows, respectively. (d) Emission spectra of the upconversion nanoparticles (measured) and a microcrystalline $NaYF_4$:Er^{3+}(2%),Yb^{3+}(18%) sample (reference). Subtracting the reference spectrum from the nanoparticle spectrum gives the difference spectrum revealing the spectral shape of the $^2H_{9/2}$ emission.

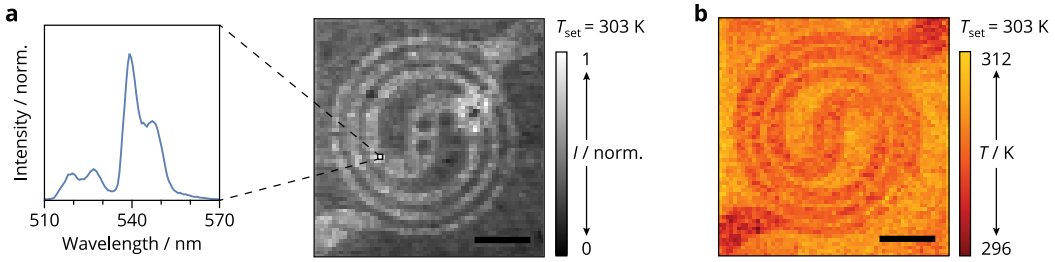

Figure 4. Temperature mapping. (a) Map of the integrated green luminescence from a microheater coated with upconversion nanoparticles at a set temperature of 303 K measured in an ambient atmosphere. The intensity of the 980 nm excitation light was 1.0 kW cm^{-2}. The measurement provides a spectrum for every pixel. The scale bar is 50 μm. (b) Converting the ratio of the emission peaks using the calibration spectra shown in Figure S1 yields a temperature map.

$^2H_{9/2}$ emission becomes stronger in the upconversion spectrum at a higher excitation intensity. This is consistent with a $^2H_{9/2}$ population mechanism requiring upconversion of three 980 nm photons compared to the two photons that were needed to populate the $^4S_{3/2}$ and $^2H_{11/2}$ levels (Figure 3c and Figure S2). As the $^2H_{9/2} \rightarrow {}^4I_{13/2}$ upconversion emission partially overlaps with the emission from the $^4S_{3/2}$ state, we must take care when integrating the spectral bands to determine the LIR. If we naively integrated between the wavelength boundaries of the $^2H_{11/2}$ and $^4S_{3/2}$ emissions (Figure 2d), we would overestimate the $^4S_{3/2}$ intensity at higher excitation powers and therefore, using eq 1, underestimate the temperature. A possible solution would be to only integrate the part of the $^4S_{3/2}$ band without an overlap with the $^2H_{9/2}$ emission, effectively excluding data points. As the relative error on a measurement of photon counts reduces with higher total counts,[27] a narrow integration boundary would thus result in a larger relative error of the LIR, leading to a higher temperature uncertainty. To maintain a low uncertainty for the measured temperature, we design a correction procedure that removes the $^2H_{9/2}$ emission.

The first step of this correction procedure is to separate the shapes of the $^2H_{11/2}$ + $^4S_{3/2}$ and the $^2H_{9/2}$ emissions via a similar approach as presented in the recent work of Rühl et al.[20] Here, we use a microcrystalline $NaYF_4$:Er^{3+}(2%),Yb^{3+}(18%) sample as a reference. This sample shows negligible $^2H_{9/2}$ emission upon 980 nm excitation at an intensity of 0.3 kW cm^{-2} (Figure 3d)[22] because the surface-to-volume ratio is much smaller compared to the nanoparticle samples. This results in a weaker coupling of $^4S_{3/2}$ with vibrations in surface species, which leads to a reduced population of $^4F_{9/2}$ and thereby results in less upconversion from $^4F_{9/2}$ to $^2H_{9/2}$.[28] The spectral difference between the reference and the luminescence that is measured from the nanoparticles then gives the shape of the $^2H_{9/2}$ emission. Using these spectral shapes, we fit a linear combination of the $^4S_{3/2}$ emission and the $^2H_{9/2}$ intensity to each experimental spectrum of a confocal map. Here, we used the same spectral range for the $^4S_{3/2}$ and $^2H_{9/2}$ emissions. Finally, we integrate the $^2H_{11/2}$ + $^4S_{3/2}$ emission between appropriate boundaries to determinate the LIR. We record reference spectra at various temperatures to apply this procedure to the calibration spectra (Figure S1) and all spectra of the temperature mapping experiments. Noticing and correcting this effect of the excitation intensity is straightforward with confocal microscopy since the measurement provides a spectrum per pixel. However, this is less straightforward with wide-field microscopy as it would require a very narrow and selective bandpass filter for the $^4S_{3/2}$ emission.

To acquire temperature-dependent luminescence from the microheater, we cover it with a layer of upconversion nanoparticles. Using a confocal microscope, we scan a 980 nm excitation laser over the microheater to acquire an array of emission spectra, which we correct using the above procedure. Integration of the $^2H_{11/2}$ + $^4S_{3/2}$ emission at each pixel yields an intensity map at a set temperature of T_{set} = 303 K (Figure 4a). Notably, the integrated luminescence is stronger on the heating spiral, indicating that the collection and/or excitation efficiency of the luminescence is higher on the metal due to its higher reflectivity. The objective used has a relatively low numerical aperture (NA) of 0.3, corresponding to a poor detection efficiency. However, its long working distance makes a large number of measurements possible, including measurements on a microheater inserted into a vacuum chamber (Figure S3a,b). To demonstrate the full potential of this setup,

https://doi.org/10.1021/acsanm.1c00657
ACS Appl. Nano Mater. 2021, 4, 4208−4215

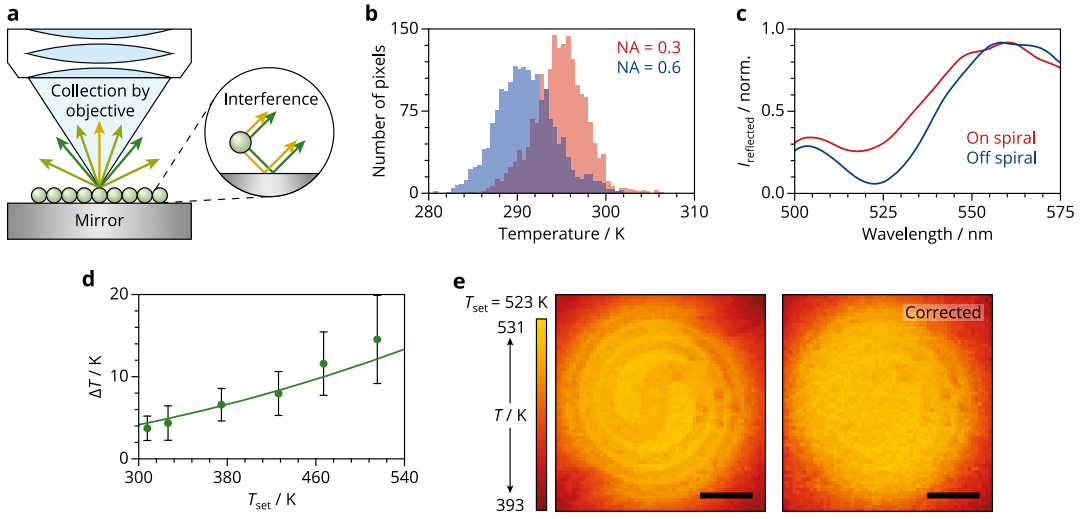

Figure 5. Artifacts in luminescence thermometry on the microscopic scale. (a) Schematic of Er^{3+}-doped nanoparticles on a mirror. Interference of the direct and the reflected $^2H_{11/2}$ (green) and $^4S_{3/2}$ (yellow) emissions changes the spectrum that is collected using the microscopy objective. (b) Histograms of the measured temperatures from 1849 pixels in the center of temperature maps that were obtained with NA values of 0.3 and 0.6 at room temperature (Figure S6). (c) Intensity of the reflected light from a halogen lamp that illuminated a location on and off the spiral of a bare microheater. The spectra were recorded with an NA of 0.75. (d) Temperature difference between locations on and off the spiral (ΔT) as a function of the set temperature. The green dots show the average of the experimental ΔT values determined from 40 pixels both on spiral and off spiral. The bars indicate the propagated errors on ΔT values determined from the standard deviation of the average apparent temperatures on and off the spiral. The solid line is a fit of the experimental ΔT values to a model that calculates the temperature dependence of the temperature error $\Delta T(T)$ from Boltzmann thermometers due to the photonic environment (eq 2). (e) Temperature map of the microheater at a set temperature of 523 K measured in an ambient atmosphere (left). The intensity of the 980 nm excitation light is 1.0 kW cm^{-2}. Correction of the left map using eq 2 yields the temperature map on the right. The scale bars are 50 μm.

we mapped the center of a microheater at 523 K in vacuum with a high pixel density (Figure S3c). In this intensity map, we can clearly distinguish the edges of the silicon nitride windows with an accuracy of ~1 μm.

Next, we convert the LIR from each corrected emission spectrum to construct a temperature map (Figure 4b). At first sight, the temperature values in the map seem to be in agreement with the set temperature. However, we notice a systematic deviation of the apparent temperature on the heating spiral—it is approximately 4 K lower. This is likely an artifact of our nanothermometry technique because the heating element cannot be colder than its surroundings. We exclude the correction procedure for multiphoton upconversion as the potential origin of this deviation since the uncorrected temperature maps show a similar trend (Figure S4). In addition, the apparent temperature did not change at different excitation intensities (Figure S5). Laser heating could therefore not be the cause of the lower apparent temperature on the heating spiral. This phenomenon thus requires further investigation to allow for reliable temperature mapping.

We propose that the systematic deviation of the apparent temperature between the spiral and the membrane is an intrinsic challenge of nanothermometry related to inhomogeneities of the photonic environment of the nanothermometers at the nanoscale.[29] Drexhage was the first to demonstrate how the emission of fluorescent molecules depends on the photonic environment, in particular, on the vicinity of a reflective mirror at a distance of up to a few times the emission wavelength.[30,31] This dependence can be explained as interference of the reflected emission with direct emission of the molecules, affecting the emission pattern (that is, the directions in which the emission is strongest) and the overall spontaneous emission rate.[32] The same interference phenomenon affected the apparent temperatures in our system. Indeed, the thickness of both the nanoparticle layer (a few μm) and the silicon nitride membrane is on the order of the emission wavelength and the microheater can act as a mirror.[33] The emission wavelengths of $^4S_{3/2}$ and $^2H_{11/2}$ are slightly different, so interference affects the emission patterns in different ways. This changes the LIR of the emission collected by our objective (Figure 5a). The different components of the microheater (metal spiral vs silicon nitride membrane) have different reflectivities, explaining why the interference effect depends on the location of the nanoparticles on the microheater.

The effect of the photonic environment becomes evident when we compare luminescence spectra acquired using objectives with different numerical apertures. We measure temperature maps of the same sample using microscopy objectives with NA values of 0.3 and 0.6. Figure 5b shows histograms of the apparent temperatures in the center of these maps, both recorded at room temperature. For a NA of 0.3, the center of the histogram is at 296 K. This value completely changes when we collect emission over a wider angle with a NA of 0.6, showing a shift to 290 K. Clearly, the dependence of the apparent temperature distributions on the NA confirms the modification of the luminescence spectrum by the photonic environment.

Further evidence of the effect of the irregular photonic environment on the microheater is obtained from reflectance measurements. Here, we study a bare microheater by separately illuminating the heating spiral and a location next to it. The intensity of the reflected light is roughly two times higher on the heating spiral (Figure S7), which is consistent with the observations shown in Figure 4a. In addition, normalization demonstrates a higher relative reflectivity on the heating spiral in the range of the $^2H_{11/2}$ emission, that is, 510−535 nm (Figure 5c). Interference between the reflected

https://doi.org/10.1021/acsanm.1c00657
ACS Appl. Nano Mater. 2021, 4, 4208−4215

and direct $^2H_{11/2}$ emissions is thus stronger on the heating spiral than off spiral.

Finally, we examine how the temperature error due to the photonic environment depends on the actual temperature in a pixel. We first determine the difference in the apparent temperature between locations on and off spiral (ΔT) and observe an increase at higher temperatures (Figure 5d). The relation between the apparent temperature and the spontaneous emission rates explains this observation (eq 1). For the nanoparticles on the microheater, we must interpret the spontaneous emission rates A_i in eq 1 as the rates of spontaneous emission under angles that can be collected by our instrumentation. This specification requires no special attention if the emission is approximately isotropic such as in thermometry on the millimeter scale where any photonic effects average out. However, nanoscale photonic heterogeneities lead to a locally different A_2/A_1 ratio. The constant C of eq 1 should therefore be multiplied by a correction factor C_p that accounts for the effect of the photonic environment on the emission rates. The apparent temperature T_p of a nanothermometer with anisotropic emission depends on its actual temperature T as well as on this correction factor C_p. This yields a temperature error of (Derivation S1)

$$\Delta T = T - T_p = T - \frac{\Delta E}{\Delta E/T + k_B \ln(C_p)} \quad (2)$$

Higher actual temperatures thus lead to an increase of ΔT for $C_p < 1$, which matches the trend shown in Figure 5d. We further confirm this by fitting the experimental ΔT values to eq 2. This gives us a method to correct the systematic deviation in measured temperatures on the microheater.

This second correction starts with the determination of C_p for each location on the microheater. Here, we assume that the temperature distribution is homogeneous for the map recorded at a set temperature of 303 K (Figure 4b and Figure S8). For every pixel, C_p is then the only unknown in eq 2, which makes it possible to construct a map of C_p values. In this case, this "calibration-free" procedure is necessary to correct the position-dependent photonic effects. We find values of around 0.95 on the spiral, while C_p is around 1 off the spiral. Indeed, the photonic effects on A_2/A_1 are expected to be subtle as the $^2H_{11/2}$ and $^4S_{3/2}$ emissions have nearly the same wavelength. To correct the maps at elevated temperatures, we plug these values and the apparent temperatures off the spiral into eq 2 to obtain the actual temperatures. The average temperature in the center of the heating spiral was lower at elevated set temperatures, up to approximately 10 K at 523 K. We attribute this deviation to a temperature gradient through the layer of nanothermometers, leading to a lower temperature near the nanothermometer−air interface than on the surface of the microheater. A potential origin of this gradient is the poor thermal conductivity of the nanothermometer layer compared to Si particles that were used for calibration of the microheater.[34] A thinner layer of nanothermometers would reduce this gradient but resulted in incomplete coverage of the microheater and it thereby complicated the analysis of the temperature homogeneity. To correct the photonic artifact, we used the apparent temperature in the center of the heating spiral as an input for the physical temperature in eq 2. After correction (Figure 5e), the microheater shows a homogeneous temperature distribution at elevated set temperatures, which matches the simulations presented in Figure 1c. This clearly demonstrates the effectiveness of our correction procedure in removing temperature artifacts due to the photonic environment.

Finally, we use the fully corrected temperature maps to study the temperature homogeneity of the microheater. Figure 6

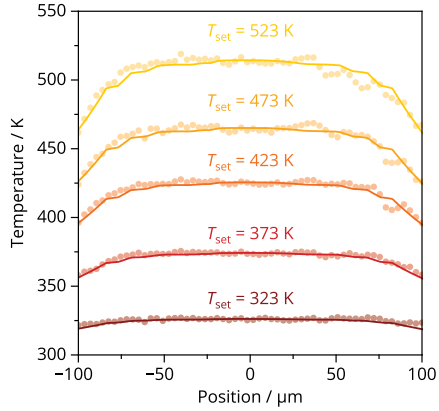

Figure 6. Mapping elevated temperatures. The dots show the average of seven horizontal line traces through the center of the temperature maps at elevated temperatures. The lines represent the temperature profiles as simulated using the finite element model.

shows horizontal traces through the center of these maps. The temperature is nearly constant in the center of these traces followed by a decrease at the edges. We compare this with temperature profiles simulated using the finite element model (Figure 1c). As an input for the simulation, we use the measured temperature at the center of the fully corrected maps. The simulated temperature profiles (lines) show an excellent match with the experimental traces (dots). We determine the standard deviation of the temperature in the center to quantify the accuracy of this thermometry method and find values of 1 K at 323 K increasing to only 4 K at 513 K. This confirms both the reliability of the finite element model as a design tool and the strength of our temperature mapping technique as a characterization tool, achieving a high accuracy and a spatial resolution of ∼1 μm. This makes nanothermometry using confocal luminescence spectroscopy a promising method to map temperature profiles in other fields such as biology[13] and catalysis,[35] where temperature variations are important but hard to monitor with conventional methods.

CONCLUSIONS

In summary, we have mapped the luminescence of upconversion nanoparticles and designed an analysis procedure to accurately measure the temperature profile of a MEMS-based microheater. To ensure high temperature accuracy, it is crucial to correct each emission spectrum for complications that are inherent to luminescence nanothermometry (but often ignored): additional emission lines at high excitation intensities and spectral variations induced by the photonic environment of the nanoparticles. A reliable correction procedure was developed and it enabled the experimental assessment of the temperature homogeneity at the surface of the microheater. The combination of luminescence thermometry and confocal microscopy not only allows for temperature mapping of this specific microheater but can also be applied to visualize temperature variations with a micrometer resolution and superior accuracy up to high temperatures in many other fields.

https://doi.org/10.1021/acsanm.1c00657
ACS Appl. Nano Mater. 2021, 4, 4208−4215

This makes our thermometry technique a valuable new tool in characterizing temperature distributions on the micrometer scale, which becomes increasingly important with the ongoing trend toward further miniaturization of devices.

■ ASSOCIATED CONTENT

Supporting Information

The Supporting Information is available free of charge at https://pubs.acs.org/doi/10.1021/acsanm.1c00657.

Further details on the relation between the $^2H_{9/2}$ emission and the excitation intensity followed by additional spectroscopic measurements of the micro-heater under various conditions and at different locations, with a derivation of eq 2 (PDF)

■ AUTHOR INFORMATION

Corresponding Authors

Andries Meijerink − *Condensed Matter and Interfaces, Debye Institute for Nanomaterials Science, Utrecht University, Utrecht 3584 CC, The Netherlands;* orcid.org/0000-0003-3573-9289; Email: a.meijerink@uu.nl

Freddy T. Rabouw − *Inorganic Chemistry and Catalysis, Debye Institute for Nanomaterials Science, Utrecht University, Utrecht 3584 CG, The Netherlands;* orcid.org/0000-0002-4775-0859; Email: f.rabouw@uu.nl

Authors

Thomas P. van Swieten − *Condensed Matter and Interfaces, Debye Institute for Nanomaterials Science, Utrecht University, Utrecht 3584 CC, The Netherlands;* orcid.org/0000-0002-1080-2045

Tijn van Omme − *DENSsolutions B.V., Delft 2628 ZD, The Netherlands;* orcid.org/0000-0002-9166-3410

Dave J. van den Heuvel − *Condensed Matter and Interfaces, Debye Institute for Nanomaterials Science, Utrecht University, Utrecht 3584 CC, The Netherlands*

Sander J.W. Vonk − *Condensed Matter and Interfaces, Debye Institute for Nanomaterials Science, Utrecht University, Utrecht 3584 CC, The Netherlands;* orcid.org/0000-0002-4650-9473

Ronald G. Spruit − *DENSsolutions B.V., Delft 2628 ZD, The Netherlands*

Florian Meirer − *Inorganic Chemistry and Catalysis, Debye Institute for Nanomaterials Science, Utrecht University, Utrecht 3584 CG, The Netherlands;* orcid.org/0000-0001-5581-5790

H. Hugo Pérez Garza − *DENSsolutions B.V., Delft 2628 ZD, The Netherlands*

Bert M. Weckhuysen − *Inorganic Chemistry and Catalysis, Debye Institute for Nanomaterials Science, Utrecht University, Utrecht 3584 CG, The Netherlands*

Robin G. Geitenbeek − *Inorganic Chemistry and Catalysis, Debye Institute for Nanomaterials Science, Utrecht University, Utrecht 3584 CG, The Netherlands*

Complete contact information is available at: https://pubs.acs.org/10.1021/acsanm.1c00657

Notes

The authors declare the following competing financial interest(s): T.v.O., R.G.S., and H.H.P.G. work for DENSsolutions B.V., a company manufacturing and marketing in situ TEM systems. The remaining authors declare no competing interests.

■ ACKNOWLEDGMENTS

This work was supported by The Netherlands Center for Multiscale Catalytic Energy Conversion (MCEC) and the NWO Gravitation Programme funded by the Ministry of Education, Culture and Science of the government of The Netherlands. F.T.R. and S.J.W.V. acknowledge financial support from The Netherlands Organization for Scientific Research NWO (Veni-722.017.002 and OCENW.-KLEIN.008). Hans C. Gerritsen and Gerhard A. Blab were also acknowledged for their useful advice and stimulating discussion.

■ REFERENCES

(1) Geitenbeek, R. G.; Vollenbroek, J. C.; Weijgertze, H. M. H.; Tregouet, C. B. M.; Nieuwelink, A. E.; Kennedy, C. L.; Weckhuysen, B. M.; Lohse, D.; Van Blaaderen, A.; Van Den Berg, A.; Odijk, M.; Meijerink, A. Luminescence Thermometry for *in Situ* Temperature Measurements in Microfluidic Devices. *Lab Chip* **2019**, *19*, 1236−1246.

(2) Cheng, Q.; Rajauria, S.; Schreck, E.; Smith, R.; Wang, N.; Reiner, J.; Dai, Q.; Bogy, D. Precise Nanoscale Temperature Mapping in Operational Microelectronic Devices by Use of a Phase Change Material. *Sci. Rep.* **2020**, *10*, 20087.

(3) van Ravenhorst, I. K.; Geitenbeek, R. G.; van der Eerden, M. J.; Tijn van Omme, J.; Peréz Garza, H. H.; Meirer, F.; Meijerink, A.; Weckhuysen, B. M. *In Situ* Local Temperature Mapping in Microscopy Nano-Reactors with Luminescence Thermometry. *ChemCatChem* **2019**, *11*, 5505−5512.

(4) Yakunin, S.; Benin, B. M.; Shynkarenko, Y.; Nazarenko, O.; Bodnarchuk, M. I.; Dirin, D. N.; Hofer, C.; Cattaneo, S.; Kovalenko, M. V. High-Resolution Remote Thermometry and Thermography Using Luminescent Low-Dimensional Tin-Halide Perovskites. *Nat. Mater.* **2019**, *18*, 846−852.

(5) Sarua, A.; Ji, H.; Kuball, M.; Uren, M. J.; Martin, T.; Hilton, K. P.; Balmer, R. S. Integrated Micro-Raman/Infrared Thermography Probe for Monitoring of Self-Heating in AlGaN/GaN Transistor Structures. *IEEE Trans. Electron Devices* **2006**, *53*, 2438−2447.

(6) Tsu, R.; Hernandez, J. G. Temperature Dependence of Silicon Raman Lines. *Appl. Phys. Lett.* **1982**, *41*, 1016−1018.

(7) Keller, E. L.; Frontiera, R. R. Ultrafast Nanoscale Raman Thermometry Proves Heating Is Not a Primary Mechanism for Plasmon-Driven Photocatalysis. *ACS Nano* **2018**, *12*, 5848−5855.

(8) Jiang, P.; Qian, X.; Yang, R. Time-Domain Thermoreflectance (TDTR) Measurements of Anisotropic Thermal Conductivity Using a Variable Spot Size Approach. *Rev. Sci. Instrum.* **2017**, *88*, 74901.

(9) Brites, C. D. S.; Balabhadra, S.; Carlos, L. D. Lanthanide-Based Thermometers: At the Cutting-Edge of Luminescence Thermometry. *Adv. Opt. Mater.* **2019**, *7*, No. 1801239.

(10) Brites, C. D. S.; Lima, P. P.; Silva, N. J. O.; Millán, A.; Amaral, V. S.; Palacio, F.; Carlos, L. D. Thermometry at the Nanoscale. *Nanoscale* **2012**, *4*, 4799−4829.

(11) Heer, S.; Kömpe, K.; Güdel, H. U.; Haase, M. Highly Efficient Multicolour Upconversion Emission in Transparent Colloids of Lanthanide-Doped $NaYF_4$ Nanocrystals. *Adv. Mater.* **2004**, *16*, 2102−2105.

(12) Vetrone, F.; Naccache, R.; Zamarrón, A.; Juarranz de la Fuente, A.; Sanz-Rodriguez, F.; Martinez Maestro, L.; Martin Rodriguez, E.; Jaque, D.; Garcia Solé, J.; Capobianco, J. A. Temperature Sensing Using Fluorescent Nanothermometers. *ACS Nano* **2010**, *4*, 3254−3258.

(13) Zhu, X.; Li, J.; Qiu, X.; Liu, Y.; Feng, W.; Li, F. Upconversion Nanocomposite for Programming Combination Cancer Therapy by Precise Control of Microscopic Temperature. *Nat. Commun.* **2018**, *9*, 2176.

(14) Piñol, R.; Zeler, J.; Brites, C. D. S.; Gu, Y.; Téllez, P.; Carneiro Neto, A. N.; da Silva, T. E.; Moreno-Loshuertos, R.; Fernandez-Silva, P.; Gallego, A. I. Real-Time Intracellular Temperature Imaging Using Lanthanide-Bearing Polymeric Micelles. *Nano Lett.* **2020**, *20*, 6466−6472.
(15) Brites, C. D. S.; Pereira, P. P.; João, N.; Millán, A.; Amaral, V.; Palacio, F.; Carlos, L. A. D. Organic-Inorganic Eu^{3+}/Tb^{3+} Codoped Hybrid Films for Temperature Mapping in Integrated Circuits. *Front. Chem.* **2013**, *1*, 9.
(16) Saïdi, E.; Babinet, N.; Lalouat, L.; Lesueur, J.; Aigouy, L.; Volz, S.; Labéguerie-Egéa, J.; Mortier, M. Tuning Temperature and Size of Hot Spots and Hot-Spot Arrays. *Small* **2011**, *7*, 259−264.
(17) Geitenbeek, R. G.; Prins, P. T.; Albrecht, W.; Van Blaaderen, A.; Weckhuysen, B. M.; Meijerink, A. $NaYF_4:Er^{3+},Yb^{3+}/SiO_2$ Core/Shell Upconverting Nanocrystals for Luminescence Thermometry up to 900 K. *J. Phys. Chem. C* **2017**, *121*, 3503−3510.
(18) Auzel, F. Upconversion and Anti-Stokes Processes with f and d Ions in Solids. *Chem. Rev.* **2004**, *104*, 139−174.
(19) Kumar, S.; Bhushan, P.; Pandey, M.; Bhattacharya, S. Additive Manufacturing as an Emerging Technology for Fabrication of Microelectromechanical Systems (MEMS). *J. Micromanuf.* **2019**, *2*, 175−197.
(20) Rühl, P.; Wang, D.; Garwe, F.; Müller, R.; Haase, M.; Krämer, K. W.; Paa, W.; Heintzmann, R.; Heinemann, S. H.; Stafast, H. Notes on Thermometric Artefacts by Er^{3+} Luminescence Band Interference. *J. Lumin.* **2021**, *232*, No. 117860.
(21) Pickel, A. D.; Teitelboim, A.; Chan, E. M.; Borys, N. J.; Schuck, P. J.; Dames, C. Apparent Self-Heating of Individual Upconverting Nanoparticle Thermometers. *Nat. Commun.* **2018**, *9*, 4907.
(22) Krämer, K. W.; Biner, D.; Frei, G.; Güdel, H. U.; Hehlen, M. P.; Lüthi, S. R. Hexagonal Sodium Yttrium Fluoride Based Green and Blue Emitting Upconversion Phosphors. *Chem. Mater.* **2004**, *16*, 1244−1251.
(23) Frederix, P. L. T. M.; Asselbergs, M. A. H.; Van Sark, W.; den Heuvel, D. J.; Hamelink, W.; De Beer, E. L.; Gerritsen, H. C. High Sensitivity Spectrograph for Use in Fluorescence Microscopy. *Appl. Spectrosc.* **2001**, *55*, 1005−1012.
(24) van Omme, J. T.; Zakhozheva, M.; Spruit, R. G.; Sholkina, M.; Garza, H. H. P. Advanced Microheater for *in Situ* Transmission Electron Microscopy; Enabling Unexplored Analytical Studies and Extreme Spatial Stability. *Ultramicroscopy* **2018**, *192*, 14−20.
(25) Saltonstall, C. B.; Serrano, J.; Norris, P. M.; Hopkins, P. E.; Beechem, T. E. Single Element Raman Thermometry. *Rev. Sci. Instrum.* **2013**, *84*, No. 064903.
(26) Renero-Lecuna, C.; Martín-Rodríguez, R.; Valiente, R.; González, J.; Rodríguez, F.; Krämer, K. W.; Güdel, H. U. Origin of the High Upconversion Green Luminescence Efficiency in β-$NaYF_4$:2%Er^{3+},20%Yb^{3+}. *Chem. Mater.* **2011**, *23*, 3442−3448.
(27) Suta, M.; Meijerink, A. A Theoretical Framework for Ratiometric Single Ion Luminescent Thermometers—Thermodynamic and Kinetic Guidelines for Optimized Performance. *Adv. Theory Simul.* **2020**, *3*, No. 2000176.
(28) Anderson, R. B.; Smith, S. J.; May, P. S.; Berry, M. T. Revisiting the NIR-to-Visible Upconversion Mechanism in β-$NaYF_4:Yb^{3+},Er^{3+}$. *J. Phys. Chem. Lett.* **2014**, *5*, 36−42.
(29) Zhou, J.; Del Rosal, B.; Jaque, D.; Uchiyama, S.; Jin, D. Advances and Challenges for Fluorescence Nanothermometry. *Nat. Methods* **2020**, *17*, 967−980.
(30) Drexhage, K. H. Influence of a Dielectric Interface on Fluorescence Decay Time. *J. Lumin.* **1970**, *1-2*, 693−701.
(31) Brechbühler, R.; Rabouw, F. T.; Rohner, P.; le Feber, B.; Poulikakos, D.; Norris, D. J. Two-Dimensional Drexhage Experiment for Electric-and Magnetic-Dipole Sources on Plasmonic Interfaces. *Phys. Rev. Lett.* **2018**, *121*, No. 113601.
(32) Ford, G. W.; Weber, W. H. Electromagnetic Interactions of Molecules with Metal Surfaces. *Phys. Rep.* **1984**, *113*, 195−287.
(33) Rabouw, F. T.; Prins, P. T.; Norris, D. J. Europium-Doped $NaYF_4$ Nanocrystals as Probes for the Electric and Magnetic Local Density of Optical States throughout the Visible Spectral Range. *Nano Lett.* **2016**, *16*, 7254−7260.
(34) Rafiei Miandashti, A.; Khosravi Khorashad, L.; Govorov, A. O.; Kordesch, M. E.; Richardson, H. H. Time-Resolved Temperature-Jump Measurements and Theoretical Simulations of Nanoscale Heat Transfer Using $NaYF_4:Yb^{3+}:Er^{3+}$ Upconverting Nanoparticles. *J. Phys. Chem. C* **2019**, *123*, 3770−3780.
(35) Geitenbeek, R. G.; Nieuwelink, A. E.; Jacobs, T. S.; Salzmann, B. B. V.; Goetze, J.; Meijerink, A.; Weckhuysen, B. M. *In Situ* Luminescence Thermometry to Locally Measure Temperature Gradients during Catalytic Reactions. *ACS Catal.* **2018**, *8*, 2397−2401.

https://doi.org/10.1021/acsanm.1c00657
ACS Appl. Nano Mater. 2021, 4, 4208−4215